Study on the Microscopic Pore Structure and Seepage Characteristics of Chang 8 Tight Sandstone Reservoir in Jiyuan Area, Ordos Basin

Bo-biao Liu[1(✉)], Cheng-qian Tan[2], Delu Li[3], Yong-qiang Zhang[4], and Rong-xi Li[1]

[1] School of Earth Science and Resources, Chang'an University, Xi'an 710054, China
`liubobiao929@163.com`
[2] School of Earth Science and Engineering, Xi'an Shiyou University, Xi'an 710065, China
`cqtan-001@xsyu.edu.cn`
[3] Shaanxi Provincial Key Laboratory of Geological Support for Coal Green Exploitation, Xi'an University of Science and Technology, Xi'an 710054, China
`Lidelu322@126.com`
[4] Changqing Oilfield Branch Exploration and Development Research Institute, Xi'an 710018, China
`yongqz@petrochina.com.cn`

Abstract. Pore structure and percolation characteristics of reservoir are very important for oilfield development. In this paper, the microscopic pore structure, movable fluid distribution and percolation characteristics of chang 8 tight sandstone reservoir were studied. The influencing factors of microscopic pore structure and seepage characteristics were analyzed. The petrological characteristics, microscopic pore structure, movable fluid distribution and percolation characteristics of the reservoir were analyzed by means of thin section observation, scanning electron microscopy, whole rock analysis, mercury injection experiment, nuclear magnetic resonance and relative permeability experiment. The results show that the reservoir is characterized by fine deviation and moderate sorting. Reservoir relative permeability curve can be divided into three types: (1) oil and water curves both are concave up, (2) oil phase is concave up, and water phase is linear, (3) oil phase is linear, and water phase is concave up. Kaolinite is beneficial to increase the percolation capacity of reservoir. Illite, illite mixed layer and chlorite are not conducive to fluid percolation. The main influencing factors of reservoir percolation characteristics are permeability, pore throat radius, pore throat sorting, pore throat connectivity. The reservoirs with high permeability, large porosity and moderate pore throat distribution have relatively low residual oil saturation, wide oil-water co-seepage area and high oil displacement efficiency in water flooding development. The movable fluid distribution and percolation characteristics of reservoir with different pore structure were compared. By comparing the distribution of movable fluids and relative permeability curve characteristics of reservoirs with different pore structures, mastering the influencing factors of seepage characteristics, and formulating

reasonable reservoir development plans for different seepage characteristics reservoir, in order to ultimately improve the reservoirs recovery.

Keywords: Tight sandstone reservoir · Microscopic pore structure · Seepage characteristics · Ordos Basin

1 Introduction

At present, the development of low permeability reservoirs accounts for an increasing proportion in China. Because of the complex pore structure, the percolation characteristics of low permeability reservoirs are quite different, and there are many contradictions in the development [1, 2]. Through the study of the microscopic pore structure and percolation characteristics, we can have a deeper understanding of the reservoir, which has important guiding significance for the development of similar reservoirs in whole Ordos Basin [3, 4].

In the stage of reservoir development, more attention has been paid to reservoir percolation characteristics, which are different from conventional reservoirs. Low permeability reservoirs are mainly manifested in the complex pore structure and seepage characteristics, and existence of Jiamin effect, which make the reservoir production more difficult and the recovery rate lower [5]. Previous studies on seepage characteristics in Jiyuan area mainly focused on Chang 4+5 and Chang 6 reservoirs. It was found that the main reasons controlling the seepage characteristics were sedimentation, diagenesis, pore structure heterogeneity, fluid properties [6–8]. Different diagenetic facies lead to different microscopic pore structure. The microscopic pore structure of reservoir controls the seepage characteristics of fluid [5]. Chang 8 reservoir is located at the bottom of Yanchang Formation, so the exploration and development is relatively late. Reservoir research is still relatively weak. Current researches focus on the source, sedimentary environment, diagenesis and reservoir physical properties [9]. There are few studies on microscopic pore structure, reservoir seepage characteristics and its influencing factors.

Through literature research, it is known that the study of reservoir diagenesis is mainly through X-ray diffraction, thin section analysis and scanning electron microscopy [2, 6]. The microscopic pore structure is mainly studied by image pore analysis, high pressure mercury injection and constant velocity mercury injection [1, 4]. Seepage characteristics are mainly studied through oil-water relative permeability experiments, water displacement experiments, and nuclear magnetic resonance experiments [5, 7]. In this paper, the diagenesis, microscopic pore throat structure and seepage characteristics are studied by thin section analysis, whole rock analysis, scanning electron microscopy, conventional physical properties, high pressure mercury injection, nuclear magnetic resonance and oil-water relative permeability experiments. According to the main controlling factors, the influencing factors of reservoir seepage ability are analyzed [10–12]. The purpose is to provide guidance for formulating reasonable reservoir development plan, and ultimately to improve reservoir recovery.

2 Geology Setting

The Ordos Basin is a superimposed basin, spanning five provinces and regions with a total area of 25×10^4 Km^2 [1–4]. Jiyuan area is located in two tectonic units of Yishan slope and Tianhuan depression (Fig. 1a) [1–3]. In recent years, under the unremitting exploration of Changqing Oilfield, Chang 8 large lithologic reservoir has been found in the lower part of Yanchang Formation (Fig. 1b). Chang 8 reservoir can be divided into Chang 8_1 and Chang 8_2 sub-layers (Fig. 1c). Core observation shows that most of the sandstones are silt-fine sandstones, mainly grey, gray-brown and gray-green. Mudstone is gray-black and dark-gray, containing plant debris and coal seam (Fig. 1c). It reflects the sedimentary period is an underwater weak-reduction to reduction environment [13]. The Sr/Ba ratio of Chang 8 formation ranges from 0.1 to 0.4, with an average of 0.24. The abundance of trace element B in mudstone ranges from 58.2 to 75.5, with an average of 65.2. This indicates that the sediment water is freshwater to brackish water. Chang 8 reservoir is a near provenance deposit [5, 7], and the provenance comes from the northwest of the basin. The reservoir is a shallow water delta deposit, sand body is mainly underwater distributary channel, and locally are estuary bar, underwater crevasse fan and sheet sand (Fig. 1c) [14, 15]. After sedimentation, the sand experienced complex diagenesis, which resulted in tight lithology, complex pore structure and serious reservoir heterogeneity, and which restricted the exploration and development of oil and gas of the study area.
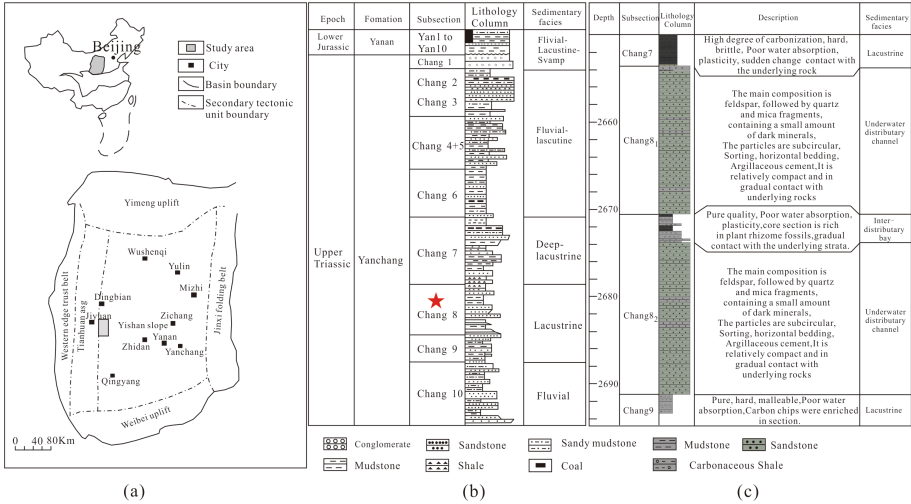

Fig. 1. Characteristics of the study area (Fig. 1a: location map of the study area; Fig. 1b: reservoir characteristics of the Triassic Yanchang Formation; Fig. 1c: reservoir inflammation characteristics of Chang8 reservoir)

3 Experimental Measurements

A series of tests were carried out on the rock plug samples collected from the core wells (2.5 cm in diameter and 2.5 cm in length). These tests include: conventional physical analysis, mineral and thin section analysis, scanning electron microscopy analysis, high pressure mercury intrusion, oil-water relative permeation experiment, nuclear magnetic resonance test.

Conventional physical analysis mainly aims at analyzing the reservoir capacity (porosity) and percolation ability (permeability) of reservoir. The experimental equipment is CM-300 and the experimental standard is SY/T5336-2006.

Thin slice analysis can observe the mineral and pore structure (pore type, throat type, throat radius) of reservoir. In order to highlight the pore characteristics filling red resin into rock slices. All kinds pore throat can be analyzed under single polarizing microscope and orthogonal microscope. Tissue staining with alizarin red and potassium cyanide can identify iron calcite, iron dolomite and non-iron calcite [2, 4].

Nineteen samples were selected for whole rock analysis and clay mineral analysis by X-ray diffraction. The X-ray diffraction experimental equipment is D5000 X-ray diffractometer [4, 6].

In order to analyze the existence type of clay minerals, thirty samples were selected for scanning electron microscopy analysis. The experimental equipment was S-4800 scanning electron microscopy (SEM) and equipped with backscatter electron detector [4].

The pore structure and pore throat distribution were analyzed by high pressure mercury injection test with 42 samples. The experimental equipment was 9505 high pressure mercury injection meter, and the maximum mercury injection pressure was 151.07 Mpa.

The oil-water relative permeability was measured by unsteady state method. Micropore adopts 100DX high pressure and high precision displacement pump (minimum flow rate 0.01 ml/min, maximum pressure 70 MPa) [16]. First, the experiment was carried out in accordance with industry standard SY/T 5345-1999. After the core is vacuumed and dried, the basic test data such as length, diameter, porosity and permeability are measured, and the effective pore volume is calculated. Second, the effective pore volume of the core is calculated by material balance method, and the salinity of the formation water is 80 000 mg/L. Third, the core is loaded into the core gripper and connected with the test system. The simulated oil (viscosity 52.6 mPa · s) is injected into the core at 70 °C, and the total amount of displaced water is measured and the irreducible water saturation is calculated. Last, constant flow mode was adopted, and the flow rate was set at 0.1 mL/min. The formation water and oil flowed out during the displacement process were measured, and the residual oil saturation was calculated as the ratio of oil-free recovery, and the test was completed [17, 18].

NMR relaxation time can be used to analyze pore throat distribution and calculate reservoir porosity, irreducible water saturation and movable fluid content. The experimental equipment of NMR is Newmark MINI-NMR, the temperature is 32 °C and the field strength is 0.5T. Specific experimental steps and methods are as follows: drilling standard cores with diameter of 25 mm from full diameter cores; washing oil before drying standard cores; measuring permeability of standard cores by gas measurement;

weighing standard cores; vacuum standard cores; saturating formation water for standard cores; weighing standard cores after saturating formation water; calculating porosity of standard cores; and measuring permeability of saturated formation water and saturated formation water for standard cores [16, 19]. The nuclear magnetic resonance T2 spectrum of saturated and centrifuged incremental of the cores were tested, and the cut-off value of T2 spectrum and movable fluid parameters were obtained.

4   Results

4.1   Detrital Mineralogy

According to the thin section identification result of 85 samples, the reservoir is mainly lithic feldspar sandstone, having an average of 30.8% quartz, 29.6% feldspar, 23.8% debris (Table 1). The abundance feldspar and debris indicates the lower composition maturity. The grains are mainly of sub-angular to sub-round, with moderate to well sorted and medium-well structural maturity. The sedimentary environment close to provenance, and water has lower energy.

The main types of debris are eruptive, quartzite, phyllite and mica, with a minor amount of flint, cryptolite, schist, metamorphic sandstone, slate and other debris (Table 2). The average filling material is 15.8%, mainly kaolinite, iron calcite, chlorite, siliceous and illite (Fig. 2). A minor amount of dolomite, laumontite, feldspar can be seen.

Table 1. Clastic Composition of Chang 8 reservoir in study area

Quartz (%)	Feldspar (%)	Debris (%)					Average of debris (%)
		Igneous rock	Metamorphic rock	Sedimentary rock	Others	Total	
19.3–45.5/30.8	25–47/29.6	8.1	10.4	2.0	3.3	14.5–47/23.8	15.8

Table 2. Lithic fragment types of Chang 8 reservoir in study area

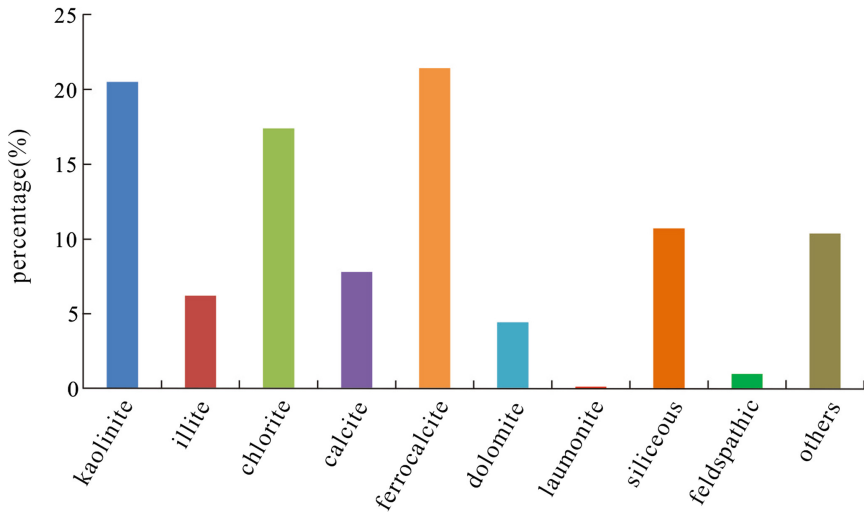| Lithic fragment types	Chert	Granite	Eruptive Rock	Aphanite	High Metamorphic Rock	Quartzite
Content (%)	1.5	0.5	29.4	2.9	1.9	12.8
Lithic fragment types	Schist	Phyllite	Metasandstone	Slate	Mica	Other Debris
Content (%)	4.7	13.2	5.0	6.0	13.7	8.5

Fig. 2. Frequency map of interstitial material

4.2 Diagenetic Minerals

With the increase of burial depth, mineralogic changes produced, which indicate the interaction between loose sediments and pore fluids [2, 4, 6]. Through thin section identification, scanning electron microscopy and whole rock diffraction analysis of rock samples, the cements are diversified, mainly porous cement, contact cements, grain-coating to porous cements, grain-coating -enlarged type cements (Fig. 3). Authigenic minerals include grain-coating and pore-lining clay minerals, pore-filling and grain replacement calcite, authigenic quartz, chlorite, illite and laumontite (Fig. 3).

The thin section results show that the reservoir has undergone compaction, cementation, metasomatism, pressure solution and dissolution. The compaction is mainly manifested by linear contact between particles, internal fracture of quartz particles and extrusion deformation of plastic particles such as mica (Fig. 3a, b) [20, 21]. Scanning electron microscopy showed that chlorite film surrounded the grain surface (Fig. 2b, c), intergranular pore filled with authigenic calcite (Fig. 3c), inter-granular pore filled with book-leaf kaolinite (Fig. 3d), filamentous illite (Fig. 3e, f), kaolinite and iron calcite filled with pore and metasomatized debris (Fig. 3g), some granular surface developed illite film, and a small amount of authigenic quartz fills the intergranular pore (Fig. 3h) [22]. The carbonate cementation is mainly composed of calcite and iron calcite (Fig. 3c, f). The laumontite is filled in the intergranular pore (Fig. 3i). Microscopically, siliceous cementation can be seen, showing secondary enlargement of quartz and development of authigenic quartz. Feldspar dissolution forms secondary pore [23], and a small amount of clastic dissolution produces
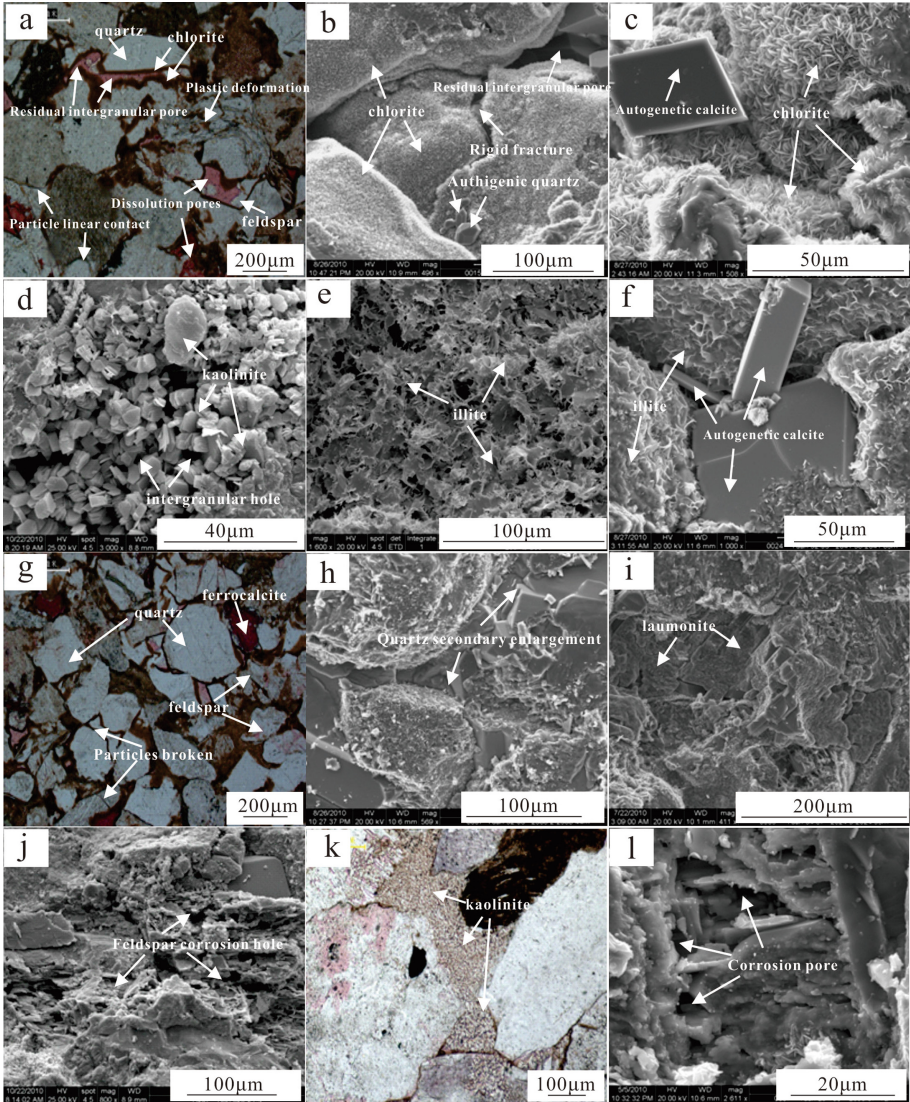
Fig. 3. a: H177, 2538.0 m, concave-convex contact of particles, partial plastic particle deformation; b: Y32-93, 2629.12, rigid particle rupture, authigenic quartz filling in cracks; c: Y32-93, 2634.8 m, authigenic calcite filled in intergranular pore throat; d: H207, 5958.0 m, clastic dissolution forms secondary pore, kaolinite and illite are distributed in intergranular pore; e: Y41-82, 2588.1 m, illite grows on the surface of particles; f: Y32-93, 2641.6 m, pore throat filled with authigenic calcite; g: H177, 2536.0 m, kaolinite and iron calcite filled with pore and metasomatized debris, a small amount of intergranular pore; h: Y32-93, 2568.2 m, quartz enlarged cemented, compact overall structure; I: Y34-87, 2624.3 m, turbidite filled with pore throat; J: H207, 2949.9 m, feldspar dissolution formed secondary pore; K: H3, 2571.4 m, kaolinite filled with full pore; L: Y29-100, 2593.4 m. a small amount of debris dissolves to produce dissolution pore.

dissolution pore (Fig. 3a, j, i). The development of dissolution pore is helpful to improve reservoir physical properties.

Quantitative analysis of rock samples by X-ray diffraction shows that the reservoirs are mainly composed of quartz (52.8%), plagioclase (21.3%), clay minerals (9.9%), calcite and siderite. Analysis results of clay minerals show that the main clay minerals
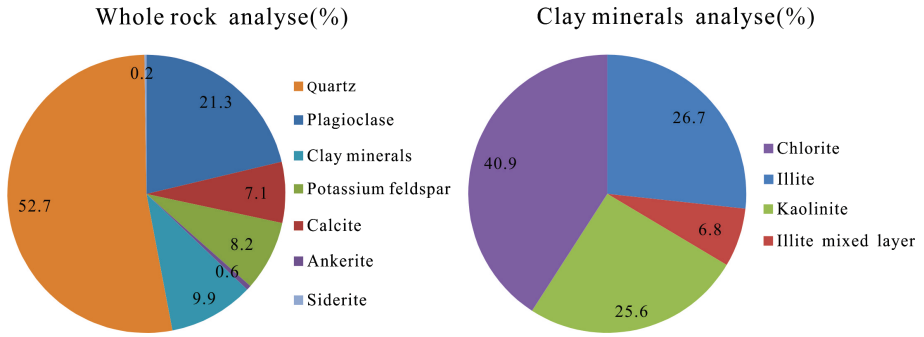

Fig. 4. Pie chart of whole rock analysis results

are chlorite (40.9%), kaolinite (25.6%), illite (26.7%) and illite mixed layer (6.8%) (Fig. 4) [24].

4.3   Physical Properties and Pore Structure

Porosity and permeability are two important parameters reflecting reservoir macro-physical properties [25, 26]. The pores are made up of intergranular pore, feldspar dissolved pore, and intragranular pore (Table 3). The conventional physical analysis results show that the effective porosity mainly distributes between 5% and 15%,
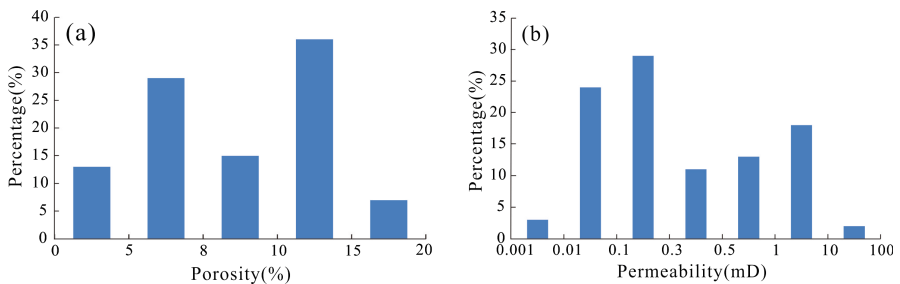

Fig. 5. Frequency map of physical property distribution

Table 3. Pore type of Chang8 oil layer in study area

Intergranular pore (%)	Feldspar dissolved pore (%)	Intragranular pore (%)	Cuttings corrosion pore (%)
58.9	33.9	6.6	0.4

averaging 7.1% (Fig. 5a), and effective permeability distributes between 0.01 mD to 10 mD, averaging 0.39 mD (Fig. 5b). According to the classification criteria of Changqing Oilfield, the reservoirs are low-porosity to ultra-low-porosity, low-permeability to ultra-low-permeability.

Quantitative Capillary Parameters:
The pore structure mainly refers to the matching characteristics of pore and throat, which determine the connectivity between pore and throat [27]. Therefore, pore structure is an important aspect of reservoir research. This paper mainly analyses reservoir pore structure characteristics by mercury injection experiments.

Table 4 is the result of core mercury injection experiment. The sorting coefficient is between 0.7–3.0 with an average of 1.6. The expulsion pressure is between 0.73–

Table 4. Pore throat characteristic parameters of Chang 8 oil layer in study area

Parameter		Max	Min	Mean
Physical properties	Porosity (%)	14.6	3.5	8.5
	Permeability ($\times 10^{-3}$ μm)	1.137	0.050	0.334
Mercury injection parameters	Mean value	13.7	9.6	12.3
	Sorting coefficient	3.0	0.7	1.6
	Variation coefficient	0.30	0.05	0.13
	Median pressure (Mpa)	37.9	0.0	9.9
	Median radius (μm)	0.34	0.00	0.11
	Expulsion pressure (Mpa)	18.70	0.73	2.31
	Maximum mercury saturation (%)	89.8	45.4	71.2
	Efficiency of mercury withdrawal (%)	47.5	21.9	36.5

18.70 Mpa, with an average of 2.31 Mpa; Median pressure is between 0–37.9 Mpa with an average of 9.9 Mpa. Median radius is between 0–0.34 um with an average of 0.11 um. The maximum mercury saturation ranged from 45.4% to 89.8%, with an average of 71.2%, and the efficiency of mercury withdraw ranged from 21.9% to 47.5%, with an average of 36.5%.

Characteristics of Capillary Pressure Curve. The shape of mercury intrusion curve is controlled by sorting and skewness. Sorting is a reaction of the degree of dispersion and concentration of pore throat distribution. The separability determines the connectivity of the pore throat. The skewness reflects the size of pore throat. The

roughness skewness is in favor of macropore throat, while the fineness skewness is in favor of small pore throat [14].

The shape of mercury injection curve and pore throat radius distribution show that mercury injection curve deviates to the fine skewness, and the overall displacement
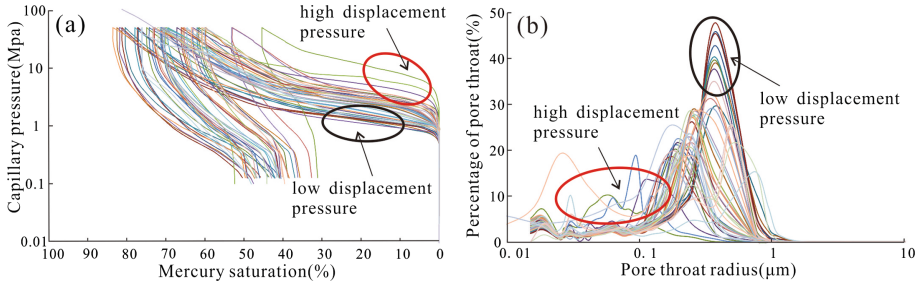

Fig. 6. The characteristic of capillary pressure curve

pressure is relatively high. The horizontal section of the intrusive mercury curve is medium length, indicating that the reservoir sorting is medium (Fig. 6a). Mercury injection experiments show that pore throat radius of reservoir mainly distributes between 0.1–1.0 um (Fig. 6b). Different samples have different mercury injection curves, corresponding to pore throat radius peak frequencies are different. (Figure 6a, b) [28].

4.4   Reservoir Seepage Characteristics

Oil-Water Relative Permeability Experiment Result. Theoretically, the physical and chemical properties of reservoirs can be reflected on the relative permeability curves [28]. Low permeability reservoirs are characterized by high irreducible water saturation, low original oil saturation, narrow oil-water co-seepage area and low oil displacement efficiency [28].

Table 5 is the characteristic parameters of the relative permeability curve, the irreducible water saturation is distributed between 29.3–43.6%, with an average of 36.0%. Residual oil saturation is high, with an average of 32.8%. The oil-water co-seepage area is distributed between 22.4% and 42.6%, with an average of 31.2%. The saturation corresponding to oil-water iso-seepage points is distributed between 40.8% and 66.0%, with an average of 55.5%, which indicates reservoir weak hydrophilicity. Relative permeability at oil-water co-seepage points are between 0.06 md and 0.18 md, with an average of 0.124 md, reflecting the strong interference between oil and water. The water relative permeability corresponding to residual oil is between 0.155 and 0.610 md, with an average of 0.326 md. The higher the permeability of reservoir, the relative permeability of water phase corresponding to residual oil is also higher. The oil displacement efficiency ranges from 33.1% to 72.4%, with an average of 49.6%.

Table 5. Relative permeability characteristic parameters of samples in study area

Well	Porosity (%)	Permeability (md)	Bound water saturation (%)	Residual oil saturation (%)	Movable oil (%)	Water saturation at the isotonic point (%)	Relative permeability at the isosmotic point (mD)	Permeability of water phase to residual oil (mD)
Y29-100-1	9.3	0.473	29.3	43.6	27.1	40.8	0.185	0.523
Y29-100-2	7.2	0.118	30.3	45.2	24.5	48.2	0.124	0.237
Y29-100-3	7.1	0.104	32.3	45.3	22.4	49.5	0.147	0.207
Y26-94	6.5	0.165	37.0	39.6	23.4	56.0	0.114	0.155
Y34-87	11.5	0.657	37.9	19.5	42.6	62.3	0.060	0.204
Y32-96	14.1	0.388	39.5	30.6	29.9	66.0	0.089	0.234
Y41-82	9.5	0.280	33.7	35.4	30.9	62.4	0.091	0.168
Y33-89	16.2	2.071	40.5	20.5	39.0	57.3	0.149	0.594
Y32-93	15.1	3.299	43.6	15.6	40.8	57.1	0.158	0.610

According to the shape of oil phase and water phase curves, the experimental results can be divided into three types. The first type is curve concave up of both oil phase and water phase (Fig. 7a). The relative permeability of oil phase decreases greatly at low water saturation, but reduce slowly during high water saturation. The relative permeability of water phase increases slowly with the increase of water saturation, and increase rapidly when water saturation is high. Residual oil saturation is less than 25%, the relative permeability at the isotonic point is 0.138 md, and the two-phase co-seepage zone is large [29–31]. It reflects that reservoir pore structure is good, heterogeneity is weak, and reservoir neutral-weak hydrophilic is dominant.

The second type is oil phase concave up and water phase straight line (Fig. 7b). With the increase of water saturation, the relative permeability of oil phase decreases rapidly at first, but slowly reduces when it reaches medium and high water saturation. While the relative permeability of water phase increases uniformly with the increase of water saturation [32, 33]. The residual oil saturation is more than 40%, the relative permeability at the isotonic point is 0.128 md, and the two-phase co-seepage zone is
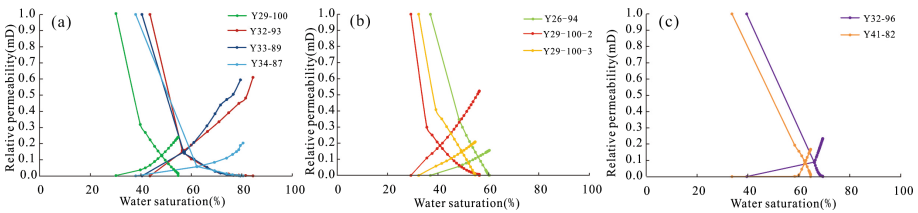

Fig. 7. Classification characteristics of relative permeability curve (Fig. 7a curve concave up of both oil phase and water phase; Fig. 7b oil phase concave up and water phase straight line; Fig. 7c oil phase linear, and water phase concave up)

narrower than the first type. The reservoir is mainly weak oil-affinity, and the pore throat radius of the reservoir is relatively small.

The third type is oil phase linear, and water phase concave up (Fig. 7c). The relative permeability of oil phase decreases evenly with the increase of water saturation, and the relative permeability of water phase increase slowly at low water cut, but In the middle and high water-cut stage, it rises rapidly. The residual oil saturation is more than 30%, and the relative permeability at the isotonic point is less than 0.1 md. The two phases interfere with each other strongly and the reservoir is hydrophilic. In the early stage, water is visible, oil production decreases slowly, reservoir pore structure is complex and heterogeneity is strong [31, 34].

Table 6. Nuclear magnetic resonance test results of samples

Sample	Depth (m)	Porosity (%)	Permeability (10^{-3}um^2)	T2cutoff (ms)	Swi (%)	Movable fluid saturation (%)
Y21	2624.4	13.7	0.7803	1.825	68.0	32.0
Y18	2665.1	13.8	0.8376	2.248	67.5	32.5
Y8	2584.1	4.0	0.0001	38.720	93.6	6.4
Y3	2608.2	5.5	0.0149	7.843	71.2	28.8
Y1	2585.4	8.1	0.2685	9.011	55.9	44.1

NMR Testing Result. NMR experiments can be used to analyze the movable fluids distribution and pore distribution of reservoirs. The experimental results show the sample porosity is distributed 4–13.8%, the permeability is distributed 0.0001–0.8376 mD. The irreducible water saturation is distributed 55.9–93.6%, and the movable fluid saturation is distributed 6.4–44.1%. The NMR pore throat radius is distributed 0.001 to 10 um (Table 6).

The porosities and permeabilities of Y18 and Y21 are higher than those of Y1, but the saturation of movable fluid is lower than that of Y1 samples, and the bound water is higher than that of Y1 (Table 6). Therefore, movable fluids are not completely controlled by physical and are closely related to pore throat characteristics of reservoirs.

Figure 8a shows the distribution characteristics of T2 spectrum when the sample is saturated incremental, which ranges from 0.04 ms to 800 ms. The morphology of T2 spectrum is bimodal, which can be divided into two categories according to the peak type: the left peak is higher than the right peak (Y18, Y21, Y3, Y8) and right peak is higher than left peak (Y1). Left peak of the samples are basically between 0.1 and 2 ms, and the peak frequencies of different samples are slightly different. The peak frequencies of Y18 and 21 are 26%, and those of Y8, Y3 and Y1 are 9.0%. The right peak of Y18 and Y21 is between 7 and 60 ms, and the peak frequency is 10.0%. The peak value of Y 8 samples is 8–40 ms and the frequency is 3.0%. The peak values of Y3 and Y1 are 70–600 ms, with frequencies of 4% and 9%, respectively (Table 6). Reflecting the micropore distribution is similar but macropore is different.

Centrifuged incremental, the T2 spectra are single peaks, with peaks ranging from 0.1 ms to 1 ms (Fig. 8b). The T2 spectra reflect the bound water distribution characteristics, which are mainly distributed in micropore throats and difficult to flow.

The accumulation curve of porosity saturated and centrifuged shows that the movable porosity of each sample is 3.6% for Y1, 1.6% for Y3, 0.3% for Y8, 4.5% for Y18 and 4.5% for Y21 (Fig. 8c). The movable fluids of the samples are all contributed
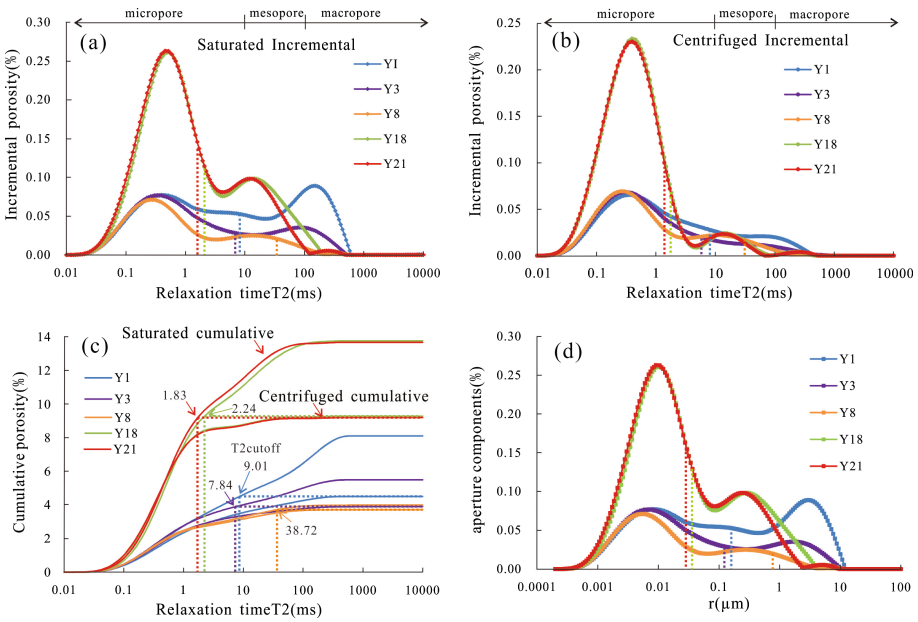

Fig. 8. Pore and throat distribution characteristics of NMR (Fig. 8a: Porosity distribution of NMR T2 spectrum saturated increment; Fig. 8b: Porosity distribution of NMR T2 spectrum centrifuged increment; Fig. 8c: Porosity accumulation distribution of NMR T2 spectrum; Fig. 8d: Pore size distribution characteristics of samples)

by the mesopore and macropore connected pore throats.

Figure 8d shows the pore size distribution from NMR samples. The pore distribution curve is bimodal, which is consistent with the saturated T2 spectrum. The pore sizes of all samples are concentrated in two regions, with slightly different distribution regions and frequencies. The distribution of micropore is basically the same, ranging from 0.005 to 0.040 um. The frequencies of Y18 and 21 are 26.0%, and those of Y8, Y3 and Y1 are 9.0%. The proportion of micropore in Y18 and 21 is large, while the large pore throat are slightly different. The pore of Y21, Y18 and Y 8 are between 0.2 to 0.8 um. The macropore of Y1 sample ranges from 1 to 10 um, and that of Y3 ranges from 0.8 to 6.0 um. According to the effective pore throat distribution (T2 cutoff), the pore throat of Y21 is 0.029 um, Y18 is 0.039 um, Y8 is 0.674 um, Y3 is 0.119 um, Y1 is 0.146 um. Movable fluid is closely related to reservoir pore structure (Fig. 8c, d).
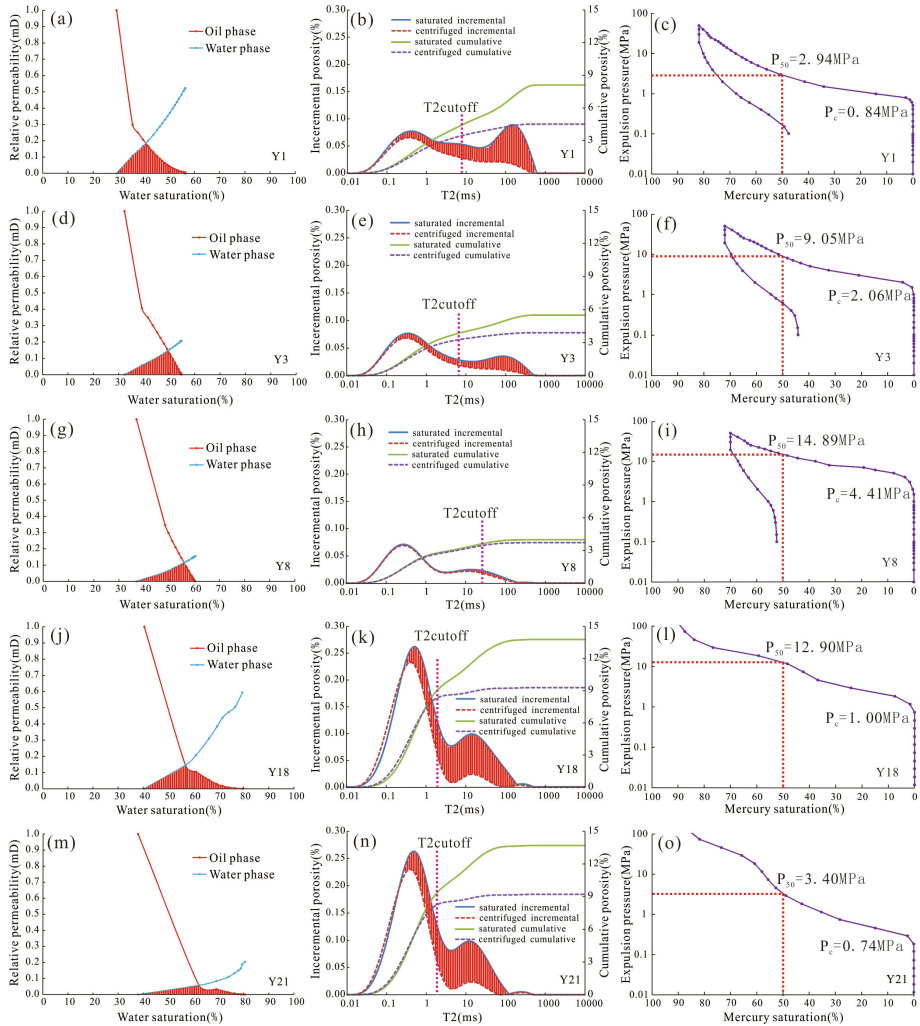
Fig. 9. Relative permeability curve -NMR T2- Mercury injection curve of samples

The relative permeability curves, NMR T2 spectra and Mercury injection curve of five different samples were compared and analyzed (Fig. 9). The oil-water co-seepage area of Y1 was the largest, the movable fluid saturation was 44.1% (Fig. 9b), and the corresponding median pressure was 2.93 Mpa (Fig. 9c). The oil-water co-seepage area of Y18 was the second, the movable fluid saturation was 32.5% (Fig. 9j), the median capillary pressure was 12.9 Mpa (Fig. 9l). The movable fluid saturation of Y21 was 32.0% (Fig. 9n), the median capillary pressure is 3.40 Mpa (Fig. 9o). The movable fluid saturation of Y8 is 6.4% (Fig. 9h), the median capillary pressure is 14.89 Mpa (Fig. 9i); Movable fluid saturation of Y3 is 28.8% (Fig. 9e), corresponding to the median capillary pressure is 9.08 Mpa (Fig. 9f). The comparison results show that the

area of oil-water co-seepage zone and movable fluid are closely related to reservoir pore structure.

Movable fluid saturation is closely related to capillary pressure curve. Sample Y1 has the highest movable fluid saturation (44.1%), which corresponds to lower displacement pressure and median pressure. The displacement pressure of Y18 and Y21 sample is close to that of Y1 sample, but the median pressure is high (Fig. 9). The corresponding movable fluid saturation is lower about 32%. The displacement pressure of Y3 sample is high, and the median pressure is medium. The volume saturation is 28.8%. The displacement pressure and median pressure of Y8 sample are relatively high, the movable fluid is 6.4%, and most of them are bound water. The saturation of movable fluid is controlled by the displacement pressure and median pressure of the sample, which shows that the maximum connected pore and segregation of reservoir control the characteristics of movable fluid.

There are many factors affecting the seepage characteristics, which are mainly including wettability, micro-pore structure and clay minerals under the same experimental conditions. When the wettability is the same, the seepage characteristics are influenced by the reservoir micro-pore structure. The smaller the displacement pressure is, the better the samples are sorted, and the smaller the interference of oil-water co-seepage flow will be. Compared with Y18 and Y21, the saturation of movable fluid is 32%, but the seepage characteristics are different (Fig. 9 j, m). The separation performance of Y18 is better than that of Y21, and the interference between oil and water phase is less. However, Y21 is poorly sorted. During the process of oil injection into reservoir, non-piston displacement will take place, water preferentially flows into larger connected pore throats, and the oil is stuck and unable to flow continuously. With the increase of water saturation, oil-water phase seepage interferes seriously with each other and the relative permeability of common seepage point is low.

5   Discussion

5.1   Diagenetic Phases and Its Evolution

Diagenesis refers to the process of interaction between sediments and pore fluids prior to metamorphism [35]. Petrological analysis, thin section identification and whole rock X-ray diffraction analysis show that the main diagenetic facies are compaction, pressure dissolution, transition, metasomatism and dissolution (Fig. 3). According to the criteria for the division of diagenetic stages of clastic rocks (SY/T5477-2003), and combining

Diagenetic stage		Ancient temperature /°C	Compaction	Quartz secondary enlargement	Authigenic quartz	Carbonate mineral						Clay minerals content				chlorite		Dissolution		Pore
						Calcite	Microcrystalline calcite	Ferrocalcite	Anhydrite	Siderite	Laumonite	Andreattite	Montmorillonite	Kaolinite	illite	Pore linings chlorite	Pore-filled chlorite	Feldspar detritus	Carbonate	
Stage	Period																			
Syngenetic stage		normal temperature																		Primary pore
Early diagenetic stage	A	normal temperature ~65																		Primary pore small number of secondary pores
Early diagenetic stage	B	65~85																		Primary pores can be retained and secondary pores developed
Mesogenetic stage	A	85~140																		Porosity decreases, and cracks and intergranular pores appear
Mesogenetic stage	B	140~175																		Fracture development

Fig. 10. Diagenetic evolution sequence of reservoir

the combined characteristics of various authigenic minerals, the Chang 8 sandstone reservoir is determined to be in the middle diagenetic stage A (Fig. 10). Based on the growth relationship of various authigenic minerals and the sequence of diagenesis, the diagenetic evolution sequence is reconstructed.

The diagenetic evolution sequence is: The mechanical compaction lasted from sedimentation to the end of early diagenesis stage, particles are in linear contact and rigid particles are broken. In early diagenesis stage A: the formation of pore-lining chlorite, siderite, montmorillonite and the quartz secondary enlarged. Early diagenetic stage B: The formation of calcite, microcrystalline calcite, kaolinite and andreattite is initiated, and feldspar and calcite began to dissolve. Middle diagenetic stage A: authigenic quartz, ferrocalcite and illite are abundant, carbonate minerals dissolution occurs (Fig. 10) [35–39].

5.2 The Relationship Between Clay Mineral and Microscopic Pore Structure

Reservoir macro physical parameters are determined by pore structure, so it is very important to study the influencing factors of micro pore structure. The samples in this study are all river sandstone samples, which ensure that the depositional environment is consistent. By analyzing the relationship between the content of clay minerals and micro-pore structure parameters, the influence of clay minerals on reservoir physical properties is clearly discussed [40]. The relationship between illite, illite mixed layer, kaolinite, chlorite and displacement pressure, median pressure, median radius and mercury removal efficiency were analyzed.

Illite content is negatively correlated with median radius and mercury removal efficiency (Fig. 11a, b). Illite content is positively correlated with displacement pressure and median pressure (Fig. 11c, d) [41]. The formation of authigenic illite during
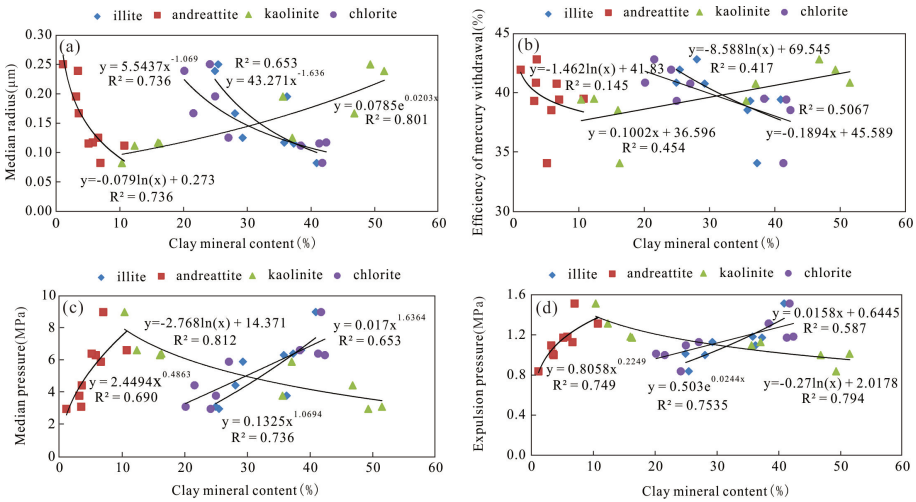
Fig. 11. Effection of clay mineral content on reservoir micropore throat parameters

diagenesis fills reservoir pore throat, reticulate and hairy shapes, which reduces the connectivity between pore throat, complicates the pore structure and has great influence on fluid seepage [42]. The higher the illite content, the worse the connectivity, the higher the pressure required in the water flooding process and the lower the oil displacement efficiency.

The increase of illite mixed layer content leads to the increase of reservoir median pressure and displacement pressure (Fig. 11c, d) [43]. With the increase of illite mixed layer content, pore throat radius and mercury removal efficiency decreases (Fig. 11a, b). The illite mixed layer adheres to the grain surface or fills in the pore with honeycomb shape, forming tiny intragranular pore in the crystal of authigenic minerals. In the process of fluid flooding, the illite mixed layer expands when it encounters water, blocking the pore, resulting in the deterioration of pore throat structure and the increase of start-up pressure [43, 44]. The illite mixed layer destroys the pore structure and physical properties of the reservoir.

The kaolinite content is negatively correlated with displacement pressure and median pressure (Fig. 11c, d) [43]. With the increase of kaolinite content, the pore throat radius and the mercury removal efficiency increases (Fig. 11a, b). A large number of kaolinite formed in the early diagenesis stage occupies reservoir pore, which makes the primary intergranular pore preserved, and there will be abundant intragranular pore in itself. In the late diagenesis stage, the unstable kaolinite undergoes dissolution and forms a large number of dissolution pore, which makes the reservoir pore better connected, the pore throat structure and the pore throat radius improved. Because reservoir connectivity is improved, so the displacement pressure and median pressure are reduced, and mercury removal efficiency is improved [43, 45]. Therefore, the existence of kaolinite is beneficial to the improvement of reservoir.

The chlorite content is harmful to the reservoir in the study area and is not conducive to the pore development. With the increase of chlorite content, reservoir median

pressure and displacement pressure increase (Fig. 11a, b). Chlorite content is negatively correlated with median radius and mercury removal efficiency (Fig. 11c, d) [46, 47]. Because chlorite exists in two kinds of reservoirs, the grain-coating chlorite formed by early diagenesis plays a supporting role in the reservoir, which is beneficial to the preservation of primary pore, and also occupies the pore and throat, making the throat radius smaller. The chlorite formed in the middle diagenesis stage plugs the pore throat, making the reservoir pore isolated, the pore throat radius smaller, and the connectivity worse. It is not conducive to the flow of fluid [43].

In reservoir diagenesis, kaolinite is beneficial to the formation of high permeability reservoir, while illite and illite mixed layers make the pore throat complex, which is not conducive to reservoir fluid seepage. Early membranous chlorite is beneficial to reservoir pore preservation, but it can destroy the percolation characteristics of fluids. Late pore filling chlorite is not conducive to pore throat development.

5.3   Influencing Factors of Reservoir Seepage Characteristics

In low permeability reservoirs, the factors affecting reservoir seepage characteristics are relatively complex, including rock physical, micro-pore throat structure and rock wettability. The shape of the relative permeability curve is the comprehensive response of the distribution state of pore fluid, pore structure characteristics [4, 7, 8]. This paper studies the influence of macrophysical properties and microscopic pore structure on reservoir seepage characteristics.

The Influence of Macroscopic Physical on Seepage Characteristics. The influence of macro physical on relative permeability characteristics is through the analysis of the
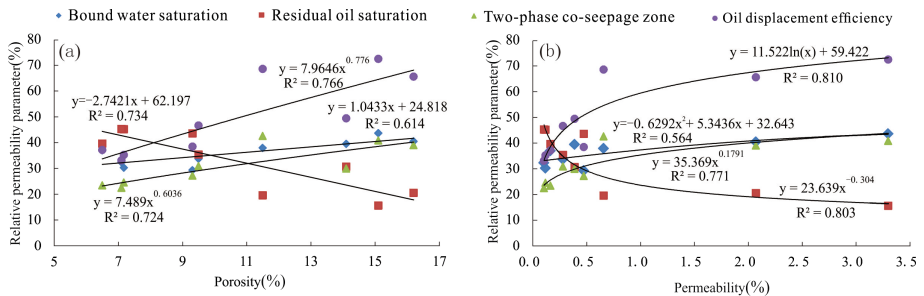

Fig. 12. Analysis of the influence of macro-physical parameters on the relative permeability parameters

correlation between reservoir physical and relative permeability parameters. Oil displacement efficiency and oil-water co-seepage zone are positively correlated with porosity and permeability. The better reservoir physical, the wider oil-water co-seepage zone, and the higher oil displacement efficiency (Fig. 12a, b). Residual oil saturation is negatively correlated with porosity and permeability, that is, the better reservoir

physical properties, the lower residual oil saturation (Fig. 12a, b). There is a weak positive correlation between irreducible water saturation and porosity and permeability (Fig. 12a, b), which is contrary to the conclusion of conventional reservoir research, is mainly due to the strong heterogeneity and complex pore structure in low permeability reservoirs. The major contribution to reservoir macrophysical is the large connected pore throat. When oil and gas fills the reservoir, it enters the larger pore throat more advanced, which makes the water in the smaller pore throat remain in the reservoir with the form of bound water. So the irreducible water saturation is high. Comparatively
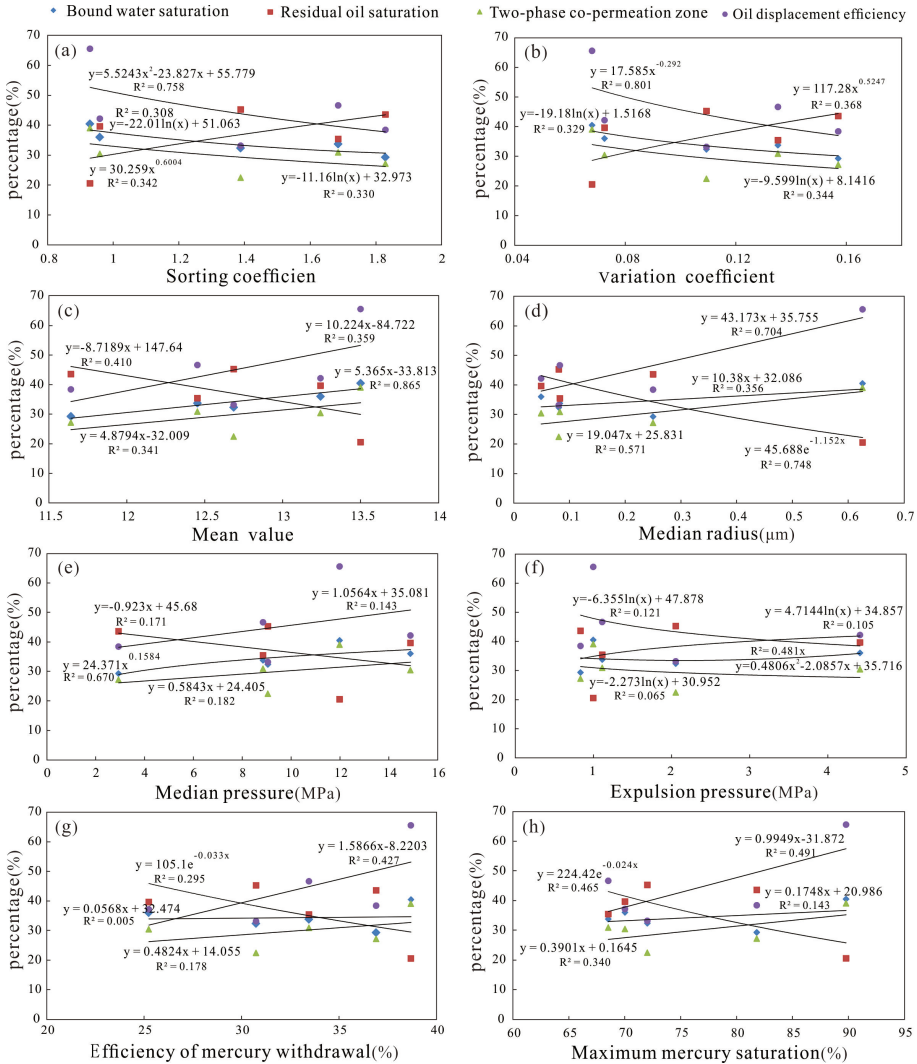

Fig. 13. Effect of micropore throat parameters on reservoir seepage characteristics

speaking, reservoir permeability has greater influence on the seepage characteristics than porosity.

The Influence of Microscopic Pore Structure on Seepage Characteristics. By analyzing the relationship between pore throat structure parameters and relative permeability characteristic parameters, the effect of pore throat structure on relative permeability is studied. There are many parameters reflecting the pore throat structure from mercury injection experiments, which reflect the pore throat size, pore throat distribution and pore throat connectivity respectively [4]. The relationship between micro pore throat structure parameters and relative permeability characteristic parameters (irreducible water saturation, residual oil saturation, oil-water co-seepage zone and oil displacement efficiency) is analyzed, and the influence of micro pore structure on seepage characteristics is determined [4, 7, 8].

The characteristic parameters reflecting pore throat distribution are sorting coefficient, variation coefficient and mean value [48]. With the increase of sorting coefficient, the residual oil saturation increases (Fig. 13a). Because of the high sorting coefficient, the reservoir heterogeneity is strong and the pore structure is complex, which makes the higher residual oil. The sorting coefficient is negatively correlated with the oil-water co-seepage zone, oil displacement efficiency and irreducible water saturation (Fig. 13a). When the sorting coefficient is high, the reservoir sortability is poor and the pore structure is complex. With the increase of sorting coefficient, the oil-water co-seepage zone becomes narrower and the oil displacement efficiency becomes lower. The variation coefficient is positively correlated with residual oil saturation, and negatively correlated with irreducible water saturation, oil-water co-seepage zone and oil displacement efficiency (Fig. 13b). Mean values is negatively correlated with residual oil saturation (Fig. 13c). The higher the mean values, the better the reservoir mean values and the lower the residual oil saturation (Fig. 13c). Mean value is positively correlated with oil-water co-seepage zone, displacement efficiency and irreducible water saturation. The higher the mean value, the wider the two-phase co-seepage zone, the higher the displacement efficiency and the higher the irreducible water saturation (Fig. 13c) [49].

The characteristic parameters of pore throat size are median radius, median pressure and displacement pressure [48]. The median radius is negatively correlated with the residual oil saturation, that is, with the increase of the median radius, the residual oil saturation of reservoir decreases (Fig. 13d). The oil-water co-seepage zone, the irreducible water saturation and displacement efficiency are positively correlated with the median radius (Fig. 13d). The larger the median radius, the better the pore structure of reservoir, and the easier the fluid flow in it, the wider the oil-water co-seepage zone, the higher the displacement efficiency and higher bound water saturation (Fig. 13d). Median pressure is negatively correlated with residual oil saturation, while it is positively correlated with oil-water co-seepage zone, oil displacement efficiency constraints and bound water saturation (Fig. 13e). The displacement pressure is positively correlated with the residual oil saturation, while the displacement pressure is weakly negatively correlated with the oil-water co-seepage zone and displacement efficiency, but the relationship between irreducible water saturation and irreducible water saturation is not obvious (Fig. 13f).

The parameters reflecting pore throat connectivity are mercury removal efficiency and maximum mercury saturation [48]. Efficiency of mercury withdrawal is negatively correlated with residual oil saturation (Fig. 13g), that is, with the increase of efficiency of mercury withdrawal, the residual oil saturation decreases, which reflecting that the better the reservoir connectivity, the easier the fluid is displaced, and the lower the residual oil saturation. Efficiency of mercury withdrawal is positively correlated with oil-water co-seepage zone and oil displacement efficiency (Fig. 13g). The wider the co-seepage zone is, the higher the oil displacement efficiency is. The relationship between efficiency of mercury withdrawal and irreducible water saturation is not obvious (Fig. 13g). Maximum mercury saturation is negatively correlated with residual oil saturation (Fig. 13h). Maximum mercury saturation is positively correlated with oil-water co-seepage zone and oil displacement efficiency, and weakly positively correlated with irreducible water saturation (Fig. 13h).

Comprehensive analysis shows that if the reservoir is well sorted, the pore throat radius is large and the connectivity is good, then the oil-water co-seepage area is wide, the oil displacement efficiency becomes high, and the residual oil saturation decreases [48]. The irreducible water saturation is affected not only by pore throat structure, but also by clay minerals and wettability of reservoir.

6 Conclusions

1. The reservoir is mainly lithic feldspar sandstone, high feldspar and low quartz, and contains more lithic debris, which indicates that the compositional maturity is low. The structural maturity is medium to good, which is the product of low energy and near provenance environment deposited close to provenance. Physical property analysis shows that the reservoirs are low-porosity to ultra-low porosity and low permeability to ultra-low permeability reservoirs.
2. The main pore types of reservoirs are intergranular pore, followed by dissolution pore. Mercury injection curves are characterized by fine deviation and medium reservoir sorting. Reservoir displacement pressure is relatively high, pore throat radius is distributed between 0.1 and 1 μm, pore throat radius is small and the corresponding peak frequency is high.
3. Relative permeability curve of reservoir can be divided into three types: the first type is oil phase concave-up type, and water phase concave-up type, reflecting the reservoir pore structure is good, and the heterogeneity is weak. Reservoir is mainly neutral-weak hydrophilic. The second type is oil phase concave up and water phase straight line, reservoir pore throat radius is relatively small. Heterogeneity is weak, reservoir is weak oil-affinity. The third type is oil phase linear, and water phase concave up, complex pore structure and strong heterogeneity. Reservoir has strong hydrophilicity.
4. Reservoir is in stage A of middle diagenesis, kaolinite formed during diagenesis is beneficial to the formation of high permeability reservoir. Illite and illite mixed layers make the pore throat of reservoir complex, which is not conducive to reservoir fluid seepage. Early film chlorite is beneficial to reservoir pore preservation, but plays a destructive role in fluid seepage characteristics. Late pore filling chlorite is not conducive to pore throat development.

5. The main factors affecting reservoir seepage characteristics are permeability, pore throat radius, pore throat sorting and pore throat connectivity. Therefore, reservoirs with high permeability, well developed macropore and moderate pore throat distribution have low residual oil saturation, wide oil-water co-seepage zone and high oil displacement efficiency, which are the main development areas of oilfields.

References

1. Yue, C., Qi, X., Yong, L., Yingchao, D., Wenjie, X.: Influence of pore structure on reservoir quality of low permeability sandstone reservoir: a case study from Chang 8 oil reservoir set in Jiyuan area. Ordos Basin. Lithol. Reservoirs **26**(05), 69–74 (2014)
2. Ma, H., Zhou, L., Zhang, X., Han, T., Li, J., Liu, G.: Diagenesis and favorable diagenetic facies of Chang8 reservoir in Jiyuan area of Ordos Basin. Pet. Geol. Exp. **35**(04), 378–383 (2013)
3. Liu, Z., Chen, Y., Liu, G.: The characteristics and controlled factors of Chang 82 reservoir in Jiyuan area, Ordos Basin. Sci. Technol. Eng. **14**(05), 211–214+222 (2014)
4. Liu, G., Bai, Y., Wang, W., Pan, S., Wang, M., Gao, X.: Pore structure of tight sand reservoir and its influence on precolation: a case of Chang 8 formation in Zhouchang area, Ordos Basin. Sci. Technol. Eng **17**(05), 29–34 (2017)
5. Yang, Y., Luo, J., Yang, J., Liu, X.: Analysis of the percolation characteristics and their influence factors on the Chang-8 sandstone reservoir in Jiyuan area. Geol. J. China Univ. **17**(02), 231–239 (2011)
6. Liang, Y.: The diagenetic characteristics and its influence on the reservoir property of Chang 4+5 in the Jiyuan area of Ordos Basin. Northwest University (2018)
7. Wang, W., Zhu, Y., Chen, D., Wei, C., Li, L., Wang, Z.: Micro-flow characteristics and influencing factors of low permeability reservoir: a case study of Chang 6 reservoir of Jiyuan area in Ordos Basin. Geol. Sci. Technol. Inf. **34**(02), 159–164 (2015)
8. Wu, T.: The pore structure and flow characteristics of Chang 4+5 reservoir in Jiyuan area of Ordos Basin. Northwest University (2014)
9. Li, Y., Li, D., Shangm, Y., Wu, X., Li, H., Li, X., Li, H.: Accumulation conditions and main controlling factors of Chang 6 reservoir in Huangling area. J. Xi'an Univ. Sci. Technol. **38**(04), 629–635 (2018)
10. Li, F.: Study on geology and development of low permeability reservoir in Dagu67 block of Dawangzhuang Oilfield. Central South University (2007)
11. Xu, S., You, L., Li, C., Liu, C., Zhao, Z.: Characterization of pore-throat structure in low -permeability reservoir from Zhuhai formation of 10 area in Wenchang a sag. J. Northeast Pet. Univ. **40**(05), 55–62+7-8 (2016)
12. Zhou, K., Sun, W., Wang, Z., Zhang, Y., Ma, Y.: Relative- permeability characteristics of tight sandstone reservoir from Shihezi 8 to Shanxi 1 members, eastern sulige gasfield. Nat. Gas Explor. Devel. **40**(05), 55–62+7-8 (2016)
13. Du, Y., Li, X., Han, X., Cao, H., Yu, X.: Sedimentary characteristics of early Permian Shanxi formation, Southeastern of Ordos Basin. J. Northeast Pet. Univ. **41**(03), 44–51+116 +7–8 (2017)
14. Xue, T., Xiao, B., Liu, Y., Lin, X., Bai, J., Chu, H.: Rearch on countermeasures for insufficient injectors of Huang-3 Chang-8 reservoir of Jiyuan Oilfield. Oil Drilling Prod. Technol. **36**(03), 100–102 (2014)

15. Yang, S., Zhang, C., Zhao, J., Guo, J., Liu, R.: Research on diagenetic evolutionary sequences of the Chang 9 oil-bearing formation in Zhenyan-Jingchuan area. Sci. Technol. Eng. **14**(12), 157–167 (2014)
16. Xu, X.: Experimental study on micro-pore structure and seepage characteristics of ultra-low permeability reservoirs in the Dongfenggang Oilfield. Pet. Drilling Tech. **45**(02), 96–100 (2017)
17. Yang, H., Zhang, J., Cao, W., Su, X.: The effect of polymer/surfactant combination system mobility control function on oil recovery: take the Kongnan reservoir of Dagang Oilfiled as research object. J. Petrochem. Univ. **29**(05), 83–89 (2016)
18. Sang, L., Yang, Z., Yang, G., Ding, C., Zhi, J.: Experimental study of biological viscosity reduction for high-viscosity heavy oil. Spec. Oil Gas Reservoirs **24**(06), 148–151 (2017)
19. Bi, Y., Xiu, J., Zhang, K., Ma, T.: Profile-control potential of polymer-producing bacteria FY-7 to heterogeneous reservoir. Spec. Oil Gas Reservoirs **25**(04), 123–128 (2018)
20. Yang, Y., Shang, Q., Tao, H., Huang, C., Yu, H.: Opportunity selection and parameter optimization of air foam flooding in low permeability reservoir taking Yanchang core sample as an example. Pet. Geol. Eng. **31**(02), 105–108 (2017)
21. Yu, J., Fu, H., Zhang, Z., Wu, A., Liu, Ni., Wen, H.: Petrophysical facies of Toutunhe formation in Fudong slope area, Junggar Basin. Oil Gas Geol. **39**(01), 129–139 (2018)
22. Yang, J., Jin, Q., Lv, C., Zhang, F., Li, Y., Hou, S., Li, F., Huang, Z.: Diagenetic evolution and its effect on physical property of Es3 reservoir in the western steep zone of Baxian depression. J. Northeast Pet. Univ. **41**(02), 23–34-34+5-6 (2017)
23. Liu, J., Ren, Z., Li, W., Hu, G.: Diagenesis and porosity evolution in the Chang 8_1 reservoirs of the Triassic Yanchang formation in the Xunyi area, Ordos Basin. Geol. Explor. **53**(02), 371–380 (2017)
24. Hu, H., Lu, Y., Tang, Q., Wang, M.: Quantitative research on the effect of diagenesis on porosity evolution of Xujiahe formation in Northeastern Sichuang Basin. Lithol. Reservoirs **26**(04), 103–109 (2014)
25. Sun, H., Luo, J., Yang, F., Qin, N., Yao, M., Gao, X.: A technology of oil- base foam underbalanced drilling for Shengbei block. Nat. Gas Explor. Devel. **38**(01), 68–72+9-10 (2015)
26. Zhou, X., Sun, W., Ren, D., Ren, Y., Li, S.: Reservoir flow units classification and evaluation of Chang6 in Jiyuan area. Petrochem. Indu. Appl. **33**(05), 39–43 (2014)
27. Cai, P., Wang, C., Liu, C., Yang, F., Xu, H., Xie, T., Yu, X., Meng, L.: Study on pore structure and quantitative parameters of the paleocene-cretaceous sandstone reservoir in Jiangling depression by SEM and mercury injection method. Rock Miner. Anal. **36**(02), 146–155 (2017)
28. Shi, Y., Hong, C., Fang, X., Zhou, F.: Sedimentary reservoir characteristics of sandstone team IIof Suweiyi formation in Kudong- Luntai area, Tarim Basin. Pet. Geol. Exp. **36**(04), 422–428 (2014)
29. Yan, K.: Residual oil distribution features in delta front reservoir during late period of super-high water content. Spec. Oil Gas Reservoirs **21**(05), 20–23+151-152 (2014)
30. Sun, X.: Study on the seepage characteristics of extra low permeability Reservoir Chang9 in Wucangpu blocK of Ordos Basin. Unconv. Oil Gas **3**(06), 77–81 (2016)
31. Wu, Z., Dong, P., Lei, G., Yang, S., Cao, N., Li, Y.: Oil-water two-phase flow rule based on lattice Boltzmann method. Fault-Block Oil Gas Field **23**(03), 338–341 (2016)
32. Meng, Y.: Experiment study of artificial fracture effect on oil-water flow in low-permeability reservoirs. Spec. Oil Gas Reservoirs **22**(01), 124–126+157 (2015)
33. Zhao, Z., Yan, B.: Effect of pore structure characteristics on the features of oil-water relative permeability curves in F Formation of Daqing Oilfield. Complex Hydrocarbon Reservoirs **7**(03), 45–47 (2014)

34. Fei, S., Yu, L., Huo, J., Zhang, G.: Comprehensive evaluation on Ma51+2 sub-member reservoirs of Lower Ordovician in Uxin Banner-Hengshan area, the Ordos Basin. Nat. Gas Explor. Dev. **40**(01), 10–16 (2017)
35. Wu, H., Zhang, C., Ji, Y., Liu, R., Cao, S., Chen, S., Zhang, Y., Wang, Y., Du, W., Liu, G.: Pore-throat size characterization of tight sandstone and its control on reservoir physical properties: a case study of Yanchang formation, Eastern Gansu, Ordos Basin. Acta Petrolei Sinica **38**(08), 876–887 (2017)
36. Wand, Y., Liu, L., Li, S., Ji, H., Li, L., Luo, Z., Xu, T.: Diagenesis and densification process of the Chang 8 interval of Triassic Yanchang formation, Western Jiyuan area. Ordos Basin. J. Palaeogeogr. **19**(05), 892–906 (2017)
37. Liang, C., Guo, J.: Diagenesis and reservoir characteristics of tight sandstones of Chang 8_1 member of Yanchang formation in Honghe oilfield. Ordos Basin. Pet. Geol. Recovery Effi. **24**(01), 57–63 (2017)
38. Li, Q., Wan, Y., Jiang, Q., Ding, X., Liu, X., Ren, Q., Gao, S., Chen, J.: Diagenesis and favourable diagenetic facies zones of the Chang-6 oil reservoirs in the Binxian-Changwu region, Ordos Basin. Sediment. Geol. Tethyan Geol. **36**(04), 21–29 (2016)
39. Yue, S., Huang, C., Yan, D., Liu, J., Li, X., Zhang, J.: Characteristics of pore evolution and its influencing factors of petrophysical properties of tight sandstone reservoir in Upper Triassic, Luoyi district. J. Central South Univ. (Sci. Technol.), **46**(01), 208–216 (2015)
40. Li, W., Niu, X., Liang, X., Zhang, Y., You, Y., Zhang, J., Zhen, J.: Diagenesis and Its influence on physical property of Chang 8 reservoir in Maling area of Ordos Basin. J. Oil Gas Technol. **36**(08), 6–11+3 (2014)
41. Pan, S., Wang, M., Wang, W., Bai, Y., Li, H., Gao, X.: Clay mineral and sensitivity analysis of Chang 8 ultra-low permeability reservoir in Jiyuan area. Unconv. Oil Gas **3**(03), 44–49 (2016)
42. Liu, G., Shi, Q., Gong, J., Qin, Z., Su, Z.: Reservoir characteristics and classification evaluation of Chang-6 formation in Xunyi area, Ordos Basin. Pet. Geol. Eng. **28**(05), 40–43 +155 (2014)
43. Wu, S., Zhu, R., Li, X., Jin, X., Yang, Z., Mao, Z.: Evaluation and application of porous structure characterization technologies in unconventional tight reservoirs. Earth Sci. Front. **25**(02), 191–203 (2018)
44. Ren, D., Sun, W., Dong, F., Hang, H., Qu, X.: Characteristics of movable fluids in the Chang 8_1 reservoir, Yanchang formation in Huaqing Oilfield, Ordos Basin and the influencing factors. Geol. Explor. **50**(03), 591–598 (2014)
45. Wang, M., Tang, H., Liu, S., Zhao, F., Li, L., Lu, H., Wang, J., Zhang, L.: Formation mechanism of differential sandstone densification modes and its impact on reservoir quality: a case study of Upper Paleozoic Permian in Eastern part of Sulige gas field, Ordos basin. J. China Univ. Min. Technol. **46**(06), 1282–1300 (2017)
46. Sun, J., Xue, J., Zeng, D., Wang, R., Wang, F., Li, H.: Deep tight reservoir characteristics and main controlling factors of Badaowan formation in the central Junggar basin. J. Northeast Pet. Univ. **41**(01), 1–10+135 (2017)
47. Wei, Q., Mi, H., Meng, L.: Influence of alkaline diagenesis on low resistance oil layer: a case study for Chang 6 formatin in Southern Zhoujiawan in Ordos Basin. Sci. Technol. Rev. **34**(09), 114–120 (2016)
48. Zhang, J., Liu, C., Zhu, G., Dong, C., Zhou, J.: Diagenesis and pore evolution of low permeability reservoirs in Junzhong 1 area. J. Yanan Univ. (Nat. Sci. Edn.) **34**(03), 49–53 (2015)
49. Qu, J., Qian, H., Li, P., You, X., Yuan, R.: Genesis of Authigenic Chlorite and Its influence on reservoir physical properties in Conglomerates of Baikouquan formation. Mahu Sag. Xinjiang Pet. Geol. **38**(05), 519–523 (2017)